A Comprehensive Experimental Investigation of Tubular Entry Flow of Viscoelastic Fluids:

Part I. Vortex Characteristics in Stable Flow

The characteristics of a vortex found at the entry of a 2:1 and 4:1 contraction for viscoelastic fluids is investigated. Two distinct flow regimes are identified in the contraction flow field: a vortex growth regime and a divergent flow regime. In the vortex flow regime, rheological forces are found to dominate the flow, with the vortex detachment length being a linear function of the Weissenberg number. In the divergent flow regime, the flow is found to diverge at the center line upstream of the vortex detachment plane, and the vortex size decreases with increasing flow rates. Inertial forces are important in the divergent flow regime. The entry flow characteristics for the 2:1 and 4:1 contraction are quantified in terms of the vortex detachment length as a function of Reynolds and Weissenberg number over the range of $0{:}2 < N'_{Re} < 200$ and $0.10 < N_{WS} < 0.7$.

P. J. CABLE

Department of Chemical Engineering
Monash University
Clayton, Victoria, Australia

and

D. V. BOGER

Department of Chemical Engineering
University of Delaware
Newark, Delaware

SCOPE

One of the most widespread and economically important flow geometries found in the polymer processing industry is the accelerative flow from a large reservoir or pipe into a smooth orifice or tube. This is the geometry of a spinneret, which is the fiber forming element in synthetic fiber production. Entry region flow is also found in the extrusion molding of plastic tube, rod and sheet products, and in the capillary rheometer, an instrument widely used for fundamental fluid property measurements.

The fundamental mechanisms governing the behavior of viscoelastic fluids in accelerative entry region flow are not completely understood. However, it is clear that at low and moderate flow rates, the entry flow is stable, and at higher flow rates, the entry flow of sufficiently elastic fluids can be disturbed by low Reynolds number instabilities, of a kind not seen for purely viscous fluids. The stable laminar entry flow is characterized by the development of large vortex flow patterns upstream of the small tube entrance, due to the nonlinear viscous fluid properties, as well as the elastic properties of the fluid. Theoretical approaches to modeling viscoelastic entry region flow are limited by formidable mathematical complexities. Experimental investigations have not been accompanied by adequate characterization of fluid properties. To quote a recent review article by White (1973), "A thorough quantitative experimental study relating basic rheological measurements to (entry) flow patterns is needed." The major objective of this investigation was to fulfill this need.

Interest in low Reynolds number instabilities in viscoelastic entry region flow stems from observations of extrudate distortion, or melt fracture, in the processing of polymer melts. It is found that above a certain flow rate in the extrusion process, the smooth extrudate surface becomes rough and irregular, even though the flow in the die is still in the laminar regime. In many cases, the occurrence of extrudate distortion can be directly related to the development of instabilities in the die entry region. While this is not the only instance of unstable laminar flow in polymer processing, it has attracted the most attention in the literature. Comprehension of the mechanisms involved will hopefully lead to a broader understanding of viscoelastic instability phenomena. Many criteria have been put forward for the onset of unstable entry region flow, but none has been directly substantiated by experimental flow pattern observations and independent fluid property measurements. In this work, the nature of the entry flow disturbances is established for viscoelastic fluids, and quantitative criteria for their inception are specified.

The investigation comprises a comprehensive study of the behavior of viscoelastic polymer solutions in the entry region upstream of abrupt circular contractions. Streak photography was used for flow pattern visualization. The fundamental properties of the test fluids were independently measured using a Weissenberg rheogoniometer. For the stable entry flow condition, quantitative flow pattern observations and point velocity measurements enabled the determination of the entry flow characteristics, which were correlated with the fundamental fluid property measurements. In the unstable flow regime, the nature of the entry flow disturbances was identified, and a quantitative criterion for the onset of unstable flow was obtained in terms of the fluid properties.

Correspondence concerning this paper should be addressed to D. V. Boger, Monash University, Clayton, Victoria, Australia. P. J. Cable is with ICI Australia, Limited, Ascot Vale, Victoria, Australia.

0001-1541-78-1534-0869-$01.35.

Part II of this paper is scheduled for publication in the *AIChE J.*, 24, No. 6 (1978).

CONCLUSIONS AND SIGNIFICANCE

A quantitative experimental study which relates basic rheological measurements to flow patterns for stable and unstable flow of viscoelastic fluids in tubular entry flow is presented. Two distinct flow regimes are identified for the stable entry flow of viscoelastic fluids: a vortex growth regime at low flow rates and a divergent flow regime at moderate flow rates. In the vortex growth regime, the characteristic secondary vortex which formed in the corner upstream of the small tube entrance increased in size with flow rate. Velocity profile development in the entry region was smooth and continuous, and the flow was fully developed at the small tube entrance. An approximate kinematic model is proposed for the vortex growth regime, yielding an explicit relationship for the axial velocity throughout the entrance region. Extensive parallels are drawn between the entry flow characteristics in the vortex growth regime observed for the polymer solutions in this study and those reported previously for polymer melts.

The divergent flow regime is characterized by an unexpected fluid deceleration at the upstream tube center line, while the secondary vortex decreases in size with flow rate. Developing axial velocity profiles in the entry region exhibited pronounced concavities, large off-center velocity maxima being separated by a local minimum at the center line. The secondary vortex characteristics for both flow regimes, for all the fluids studied, were correlated in terms of dimensionless groups based on system variables, kinematics, and independent fluid property measurements. Both a 2:1 and 4:1 contraction exhibited identical asymptotic behavior at low Reynolds numbers.

The divergent flow regime was in fact metastable, and multiple steady flow states are obtainable at the same volumetric flow rate and temperature over a limited range of conditions in the 4:1 contraction. The preferred entry flow configuration was time varying ond consisted of a spiralling disturbance to the entry flow pattern, wherein an asymmetric distortion in the upstream tube rotated about the center line with a regular frequency. Divergent flow could also occur at the same flow rate. Alternatively, for a limited number of cases, a third flow pattern was observed, consisting of a superposition of two out of phase spiralling disturbances, which resulted in a periodic pulsing flow.

The occurrence of multiple entry flow states was interpreted as an instability in the laminar entry flow. Based on quantitative flow pattern observations and independent fluid property measurements, a simple linear correlation was obtained between the critical stress ratio and the generalized Reynolds number for the onset of unstable flow for all fluids which exhibited multiple flow states in the 4:1 contraction. In the case of spiralling flow disturbances, further similarities were noted between polymer melts and solutions.

At higher throughputs, random entry flow distortions were observed. Although still in the laminar regime, the flow patterns showed little semblance of order. This phenomenon was regarded as a second-stage instability, separate from the spiralling disturbance. Under these conditions, the Uebler effect was observed, wherein a relatively large air bubble could persist in the region just upstream of the small tube entrance, rather than being swept downstream. High speed photography was used to ascertain the probable mechanisms behind this effect.

For the entire range of conditions studied, still photographs are presented to illustrate the nature of the entry flow patterns. A cine film was also used to record the time varying flow patterns. Copies of this film are available for loan.

The following specific conclusions can be made for this work: In the vortex growth regime, rheological forces dominate the flow. For contraction ratios of 2 and 4, the vortex detachment length is a linear function of Weissenberg number as

$$X = 2.5\, N_{WS}$$

For this flow condition, the velocity profile development in the entry region is smooth and continuous, and the flow is fully developed at the small tube entrance.

In the divergent flow regime, the flow diverges at the center line upstream of the vortex detachment plane, and the vortex size decreases with increasing flow rate. The developing velocity profiles exhibit severe concavities, off-center velocity maxima being separated by a local minimum at the center line. The velocity profile at the small tube entrance approaches uniformity.

The entry flow characteristics for both geometries may be quantified in terms of the secondary vortex detachment length as a function of Reynolds and Weissenberg numbers, for all the fluids studied, over the range $0.2 < N'_{Re} < 200$ and $0.10 < N_{WS} < 0.77$.

The divergent flow regime is metastable, and multiple steady flow states occur at the same flow rate. The preferred entry flow configuration in the 4:1 contraction is time varying, consisting of a spiralling disturbance to the entry flow pattern. The frequency of the disturbance is regular, increasing with flow rate, and is approximately inversely proportional to the fluid relaxation time.

Criteria for the inception of spiralling flow, based on quantitative flow pattern observations and independent fluid property measurements, show that to a first approximation the critical stress ratio is a linear function of the generalized Reynolds number as

$$\left.\frac{N_1}{\tau}\right|_c = 5 + 0.07\, N_{Re,\,\mathrm{gen}/c}$$

At higher throughputs in the laminar entry flow regime, a second-stage flow instability develops. The entry flow patterns become subject to random violent distortions. High frequency, nonperiodic disturbances to the secondary vortex are accompanied by almost complete stagnation of the flow in the center of the tube.

Under the conditions at which the random distortions to the entry flow occur in the 4:1 contraction, the Uebler effect is observed, wherein a relatively large air bubble remains trapped for some time in the semistagnant region of the small tube entrance before eventually being swept downstream.

Extensive reviews are available which describe the significant volume of work which has appeared in the past 20 yrs concerned with the various aspects of laminar entry flow into a tube (Dennison, 1967; Den Otter. 1970; White, 1973; Petrie and Denn, 1976; Cable, 1976). The behavior of Newtonian fluids in hydrodynamic en-

trance regions has been well established by theoretical analysis and experimental studies. However, a need does exist for clarification of the behavior of highly shear thinning inelastic fluids in real contractions and at low Reynolds numbers. Numerical solutions of the equations of motion using constitutive equations more realistic than the power law model would be useful so that nonlinear viscous effects could be separated from fluid memory effects in viscoelastic entry flows.

Theoretical approaches to the behavior of viscoelastic fluids in tubular entries have been limited by formidable mathematical complexities, which have resulted in over simplified constitutive and kinematic approximations. The first theoretical attempt which examines the influence of high elasticity on flow through abrupt changes in geometry has just appeared (Perera and Walters, 1977). Other analyses have largely relied on perturbation techniques where only slight deviations from inelastic behavior have been investigated. The experimental investigations, which are summarized in Table 1 for polymer melts and solutions, in general have either failed to adequately characterize the fundamental properties of the test fluid or to quantify entry flow pattern observations. However, it is clear that at low and moderate flow rates, the entry flow is stable, and at higher flow rates, the entry flow of sufficiently elastic fluids can be disturbed by low Reynolds number flow instabilities. Stable laminar entry flow is characterized by the development of large vortex flow patterns upstream of the small tube entrance, due to the nonlinear inelastic fluid properties. as well as elastic properties of the fluid. The characteristics of this vortex and how it is related to the fundamental flow properties and the kinematic variables are not understood.

Entry flow instabilities have been observed in most polymer melts and solutions and appear to develop in two stages. Regular, spiralling or oscillating distortions occur at relatively low flow rates. At higher throughputs, the disturbances become random and chaotic, with material of different deformation histories alternately entering the downstream tube. Of fundamental and practical

TABLE 1. EXPERIMENTAL INVESTIGATIONS OF TUBULAR ENTRY FLOWS

Polymer melts

Investigator	Year	Material	Entry geometry	Flow visualization method
Tordella	1957	LDPE	Flat entry, $\beta = 32$	Carbon black tracer, cine film
Clegg	1958	LDPE, HDPE	Flat and conical entries	Colored core, cine film
Schott and Kaghan	1959	LDPE	Flat entry, $\beta = 5.3$	Colored layers, cine film
Bagley and Birks	1960	LDPE, HDPE	Flat entry, $\beta = 20$	Carbon black threads, cine film
Bagley and Schreiber	1961	LDPE	Conical entry, 20-180 deg	Carbon black threads, cine film
Tordella	1963	LDPE, HDPE	Flat and 20 deg conical entry	Flow birefringence, cine film
Insarova	1969	Polystyrene	90 deg, 180 deg slit entry	Flow birefringence
Ballenger and White	1970	LDPE, HDPE, PMMA, polystyrene, polypropylene	Flat entry	Colored threads, cine film
Den Otter	1970	Linear and branched PDMS	Flat slit entry	Carborundum, still photo
Ballenger et al.*	1971	LDPE, HDPE, polystyrene, polypropylene	Flat entry, $\beta = 7$	Colored threads, cine film
Vinogradov et al.	1972	Polybutadiene	Flat slit entry	Stained glass particles, flow birefringence
Han and Drexler	1973	HDPE, polystyrene, polypropylene	Flat, 60 deg tapered	Streak photography
Oyanagi	1973	HDPE	Flat entry, $\beta = 11$-26	Section solidified plug, or flow birefringence

Polymer solutions

Investigator	Year	Material	Entry geometry	Flow visualization method
Vinogradov and Manin	1964	Al napthenate/gasoline	60 deg, 180 deg slit entry	Polarized light, still photo
Giesekus	1968	PAA/H_2O, 1.6-4% PIB/decalin, 4%	Flat die entry 60 to 180 deg slit entry	Streak photography
Metzner et al*	1969	PAA/H_2O, 0.5%	Reentrant tube	Streak photography
Boles et al.	1970	PIB/mineral oil, 2.5%	Flat die entry	Flow birefringence
Ballenger and White	1970	PIB/mineral oil, 2.5%	Flat die entry, $\beta = 21$	Carbon black tracers
Ballenger et al.*	1971	PIB/mineral oil, 2.5%	Flat die entry, $\beta = 21$	Carbon black tracers
Boger and RamaMurthy*	1972	Methocel/H_2O, PAA/H_2O	Flat die entry, $\beta = 2$	Streak photography
Oliver and Bragg	1973	PAA/H_2O	Flat die entries	Dye tracers, still photo
Pearson and Pickup	1973	PAA/glycerine-H_2O	Flat die entry flat tapered slit entries	Streak photography
Tomita and Shimbo*	1973	PEO solutions, 2 5-3.5%	Flat die entry	Not specified
RamaMurthy	1974	PAA/glycerine-H_2O, 1.5%	Flat die entry	Streak photography
Southern and Paul	1974	Fractionated polystyrene/benzene	Flat die entry	Flow birefringence
Strauss and Kinast	1974	PAA/H_2O, 0.12%	Tapered slit entry	Streak photography
Busby and MacSporran	1976	PAA/H_2O	Reentrant tube	Laser dopplermeter

* Results accompanied by some independent fluid property measurement.

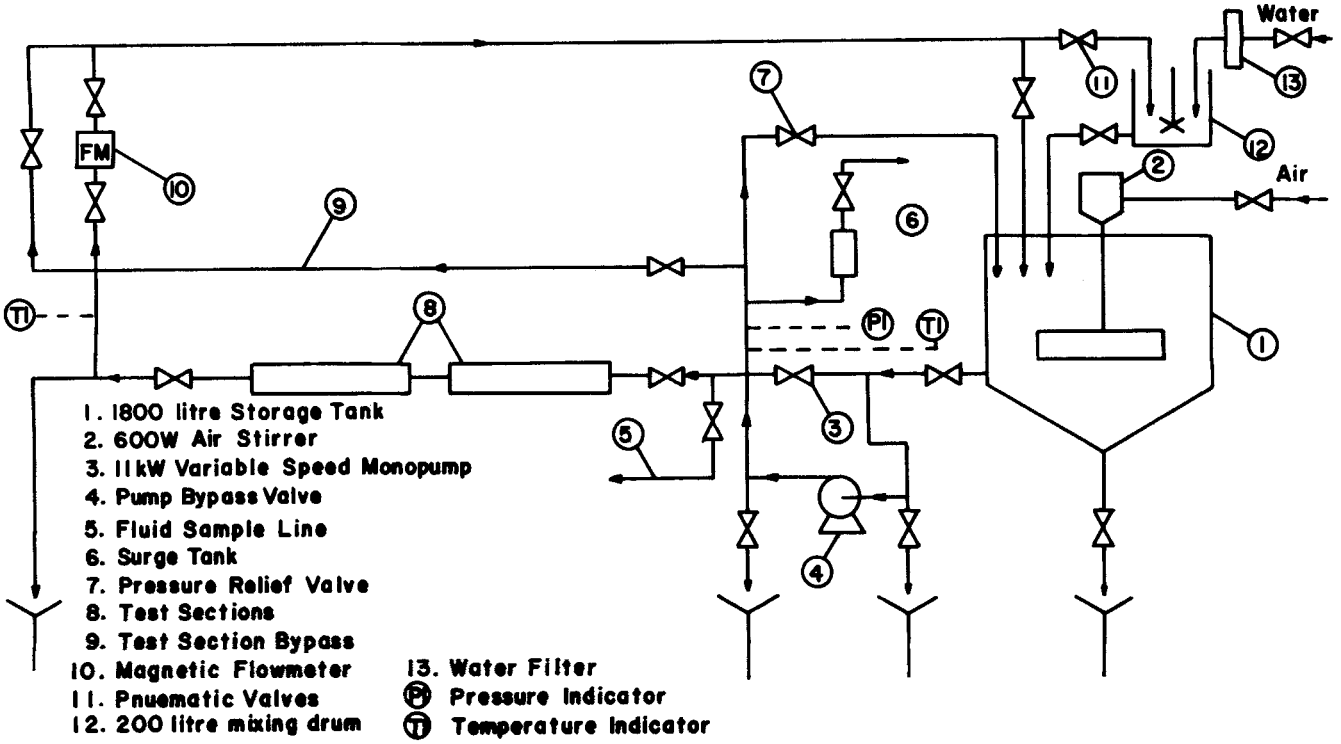

Fig. 1. Schematic diagram of flow system.

interest is when these flow patterns are to be expected, and how criteria for their inception are related to fundamental fluid properties, geometry, and kinematic variables.

This paper reports on a comprehensive experimental investigation of tubular entry flow of viscoelastic fluids. The results are presented in three parts. Part I deals with a discussion of the quantitative characteristics of the secondary flow vortex. Part II examines the velocity field on the upstream side of the contraction, and Part III deals entirely with unstable flows.

EXPERIMENTAL TECHNIQUES AND APPARATUS

Experiments on the entry flow behavior of viscoelastic fluids were carried out in a closed loop flow system, using aqueous polymer solutions as test fluids. The fluids were independently characterized using an R-16 Weissenberg Rheogoniometer. It is the purpose of this section to describe the apparatus and techniques associated with these experiments.

Flow Loop and Test Sections

A schematic diagram of the flow loop used in this study is shown in Figure 1. An 11 kW variable speed monopump was used to circulate the test fluids through two transparent test sections from an 1800 l storage tank, which was fitted with a 600 W air stirrer. A magnetic flowmeter was used to measure volumetric flow rate, and copper constantan thermocouples were used to measure the fluid temperature at the inlet and outlet of the test sections.

Two test sections were fitted in series, each containing an abrupt contraction in pipe diameter. Both were optically clear to enable visualization of flow patterns in the entry region. In one, a sudden change from a 2 to a 1 in. diameter tube was employed. The second test section, mounted downstream of the first, contained a suden 4:1 change in tube diameter, from 2 1/4 to 9/16 in. Relatively long calming lengths were included upstream of the contracting plane in each test section to allow dissipation of upstream disturbances before the entry region was reached. For the 2:1 contraction, a 5 ft length of 2 in. tubing (that is, 30 diam) was included for flow calming, and for the 4:1 system, a 6 ft length of 2 1/4 in. conduit (that is, 32 diam) was provided by means of copper pipe between the two test sections.

Optical System

The flow visualization studies entailed both the recording of flow patterns and the measurement of point velocities. Streak photography was selected as the technique, since it has been used successfully in the past for these applications (Atkinson et al., 1967; Giesekus, 1968; RamaMurthy, 1970, 1974; Halmos, 1973). The illumination of a cross section of the flow field, using a thin collimated light beam, enables the visualization of flow patterns when small, highly reflective tracer particles are suspended in the fluid. When a photograph is taken of the flow field, perpendicular to the plane of illumination, the lines produced on the negative as tracer path images are called streak lines. Streak lines approximate fluid particle path lines when small, neutrally buoyant tracer particles are used.

The tracer particles employed were Mearlite LBU, a bismuth oxychloride compound, and Timica Sparkle, which contained titanium dioxide coated mica flakes. The Timica was used in the latter stages of the investigation and gave better photographic images.

A viewing box surrounded part of each test section. The box was constructed of black anodized aluminium and could be moved on separately mounted rails up and down the length of the test section to permit observation of various sections of the flow field. Collimated light entered the bottom of the box, as a vertical sheet, through adjustable slits and an optically flat glass window. The slits were adjusted so that only the central cross section of the flow field was illuminated. The viewing box was filled with distilled water, surrounding the test section, to minimize refractive effects at curved surfaces. The front of the viewing box contained an optically flat glass window, through which the illuminated cross section of the flow field could be viewed and photographed. Attached to the bottom of the box was the optical system which focused and collimated the light sources which were employed.

The optical system was designed to fulfill two separate requirements. A continuous light source was used for recording flow patterns as streak photographs. For point velocity measurements, a double flash technique (Halmos, 1973) was used, wherein two flash tubes were triggered with an electronically preset time delay (1 to 100 ms) between them. The camera shutter was open during the flash triggering period so that flashes produced two cometlike images on the photograph. The clearly defined head of each image was used as a reference for accurate measurement of the distance traveled by the tracer

particle during the time interval between the two flash triggerings.

For still photography, a single reflex 35 mm Exacta camera fitted with a 50 mm lens was mounted on an adjustable carriage in front of the viewing box. Cine film studies were carried out using a 16 mm Pentaflex AK16 cine camera fitted with a 15 to 20 mm zoom lens and mounted on a tripod in front of the viewing box. Full details of the optical system and photographic techniques are available (Cable, 1976).

Test Fluids

The test fluids were almost exclusively aqueous solutions of Separan, a high molecular weight partially hydrolyzed ionic polyacrylamide. Two different polymer grades were employed, namely AP 30 and MG500, with a concentration range of 0.4 to 2.0% w/w. One of the test fluids also contained Carbopol 961, a carboxy polymethylene. Aqueous Separan solutions have been used extensively in previous studies of viscoelastic fluid flow as they offer good stability, high viscoelasticity, and seem to be free from thixotropic effects. One of the special advantages of Separan solutions for flow visualization work is the good optical clarity that is maintained, even at relatively high solute concentrations. The test fluids were designated by code numbers F1, F2, F3, and so on, for those used in the flow visualization experiments, and V1, V2, etc., for velocity measurement experiments.

Characterization of Test Fluids

The test fluids were characterized using an R-16 model Weissenberg Rheogoniometer (WRG) in steady rotational mode, with a cone and plate geometry. Measurements of the torque on the upper platen and the total normal thrust on the lower cone enabled calculation of the shear stress (τ) and first normal stress difference (N_1) as a function of shear rate (γ) (Walters (1975)). The characterizations were carried out under controlled temperature conditions, within ± 0.2°C of the temperature which existed in the flow loop.

A general nonlinear regression analysis program (Coulter, 1970) was used to determine power law and Ellis model parameters to give a least-squares fit of these models to the experimental data for τ and N_1 as a function of τ. The specification of model parameters for the shear stress-shear rate data allows the calculation of Reynolds numbers for the flow loop experiments from

$$N'_{Re} = \rho \frac{D^n V^{2-n}}{K} \tag{1}$$

Knowledge of the model parameters also permits calculation of the fully developed velocity profile. From the first normal stress difference and shear stress the Weissenberg number, stress ratio, and Maxwell relaxation time can be calculated as a function of shear rate:

$$N_{WS} = \frac{\theta V}{D} \tag{2}$$

$$S = \frac{N_1}{\tau} \tag{3}$$

$$\theta = \frac{N_1}{2\tau\dot{\gamma}} \tag{4}$$

A more detailed discussion on experimental methods, procedures, and data reduction is available in the original thesis (Cable, 1976), where a complete listing of the flow properties of all test fluids can be found.

Accuracy of Fundamental Flow Property Measurements

A nonlinear test sample from the National Bureau of Standards (NBS) designed for standardization of normal force measurement techniques (Kearsley, 1973) was characterized on the WRG as a check on the accuracy of the fluid property measurements. The results for shear stress and first normal stress difference are shown in Figure 2. Also shown on the same graph are some representative data, obtained by other laboratories, supplied by Kearsley (1974). Both sets of data were obtained at 25 ± 0.5°C. The shear stress data measured on R-16 WRG are slightly higher than the data supplied, and the N_1 data slightly lower, but it has been concluded that there is

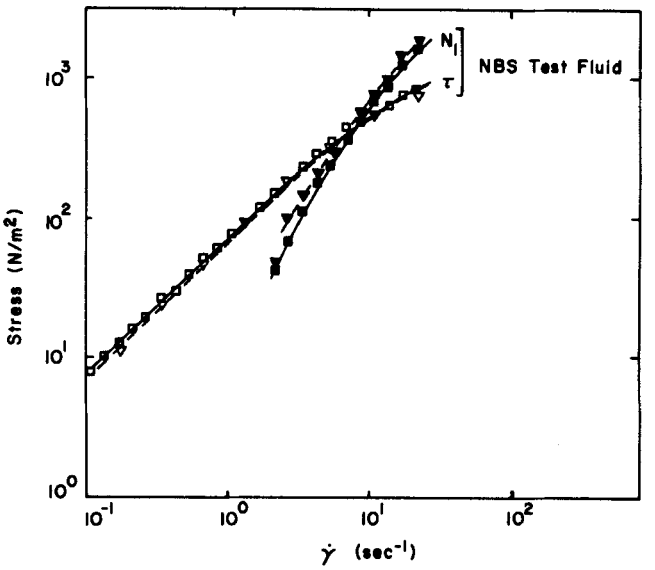

Fig. 2. Shear stress and first normal stress difference vs. shear rate for NBS fluid.

acceptable agreement of the experimental data with that supplied, and this may be interpreted as a verification of the fluid property measurements.

The reproducibility of the data was checked by characterizing one of the test fluids, V3 (F7), using two different cone angles, namely, 2 deg 1 min 26 sec and 1 deg 13 min 39 sec. The fluid was characterized with the larger cone angle, the platens

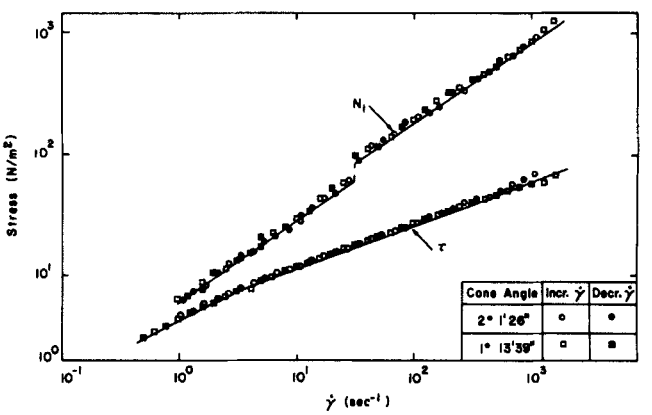

Fig. 3. Shear stress and first normal stress difference vs. shear rate for fluid V3(F7), measured using two different cone angles on the WRG.

were changed and realigned to obtain the second characterization on the same day. The results of the two sets of measurements are shown in Figure 3 as τ and N_1 vs. $\dot{\gamma}$. In Figure 3, the open circles and squares represent measurements taken with increasing shear rate, while the closed symbols denote decreasing shear rate. Also shown are the regression analysis fits of Ellis model to shear stress and two separate power law models to the first normal stress difference data. It is apparent that the two different cone angles give the same $\tau - \dot{\gamma}$ and $N_1 - \dot{\gamma}$ results, which is a significant justification of the experimental techniques. The models fit the experimental data very well. The fluid shows no time dependent effects in either shear stress or first normal stress difference, since the increasing and decreasing shear rate data are in excellent agreement with each other. An apparent discontinuity in the first normal stress difference, at $\dot{\gamma} \simeq 30\ s^{-1}$, is observed in both geometries. This is a material phenomenon which is discussed in depth elsewhere (Boger and Cable, 1977).

Comparison of Solution Properties with Polymer Melts

Since the test fluids were being used to elucidate the nature of entry flow behavior of viscoelastic materials, and a consid-

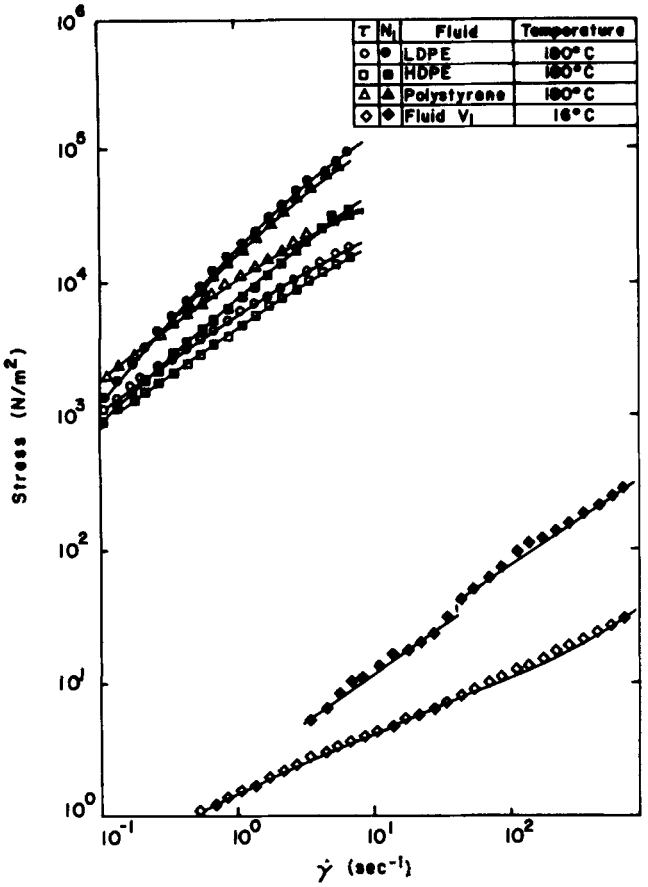

Fig. 4. A comparison of the viscometric functions for three polymer melts at 180°C and one polymer solution, fluid V1, at 16°C.

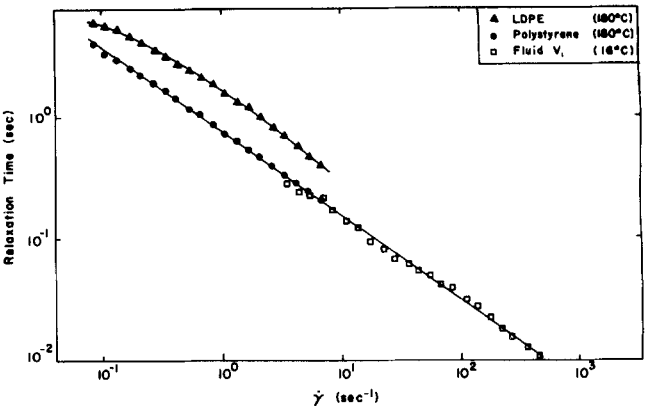

Fig. 5. A comparison of the Maxwellian relaxation time for two polymer melts at 180°C and one polymer solution, fluid V1, at 16°C.

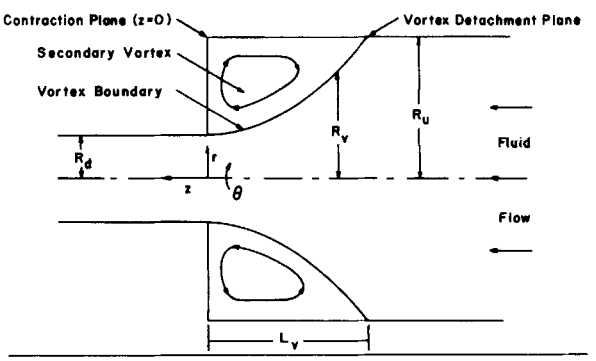

Fig. 6. System geometry for entry flow studies.

erable number of previous investigations have studied polymer melts rather than solutions, it is important to establish what rheological similarities exist between the aqueous solutions used in this work and the melts used in previous studies. Shear and normal stress data obtained by Chen (1971) may be used as an approximate indication of the rheological characteristics of the three most commonly studied melts, LDPE, HDPE, and polystyrene. The data for the three polymer melts, at 180°C, are compared in Figure 4 with those obtained for one of the test polymer solutions at 16°C. The melts exhibit significantly higher stress levels, up to four orders of magnitude larger than the polymer solution at comparable shear rates. The Maxwellian relaxation time (θ) is compared in Figure 5. It would appear that the polymer solution represents a reasonable extrapolation of the polystyrene data for higher shear rates (if the apparent negative power law dependence of θ on γ persists). The relaxation time data for the other fluids used in this study fall in a band about the line shown in Figure 5. At low shear rates, the band is quite narrow, of the order of $\pm 20\%$, which broadens to about $\pm 40\%$ for $\dot{\gamma} > 100\ s^{-1}$. Based on consideration of the relaxation time data alone, it would appear that the polymer solutions used in this study represent a reasonable model for polymer melts at higher shear rates, where flow instabilities have been observed. One of the major differences is the much lower viscosity level in the solutions, which may lead to significant inertial effects.

STABLE ENTRY FLOW-VORTEX CHARACTERISTICS

A schematic diagram of the contracting flow field is shown in Figure 6. The origin of coordinates is shown at the center of the contraction plane. A sketch of the vortex shape is included to illustrate the detachment plane, defined as the z coordinate where the flow detaches from the upstream tube wall. R_u and R_d are the radii of the upstream and downstream tubes, respectively. R_v is the radius of the converging flow zone, or vortex region, that is, the radial distance from the tube centerline to the secondary vortex boundary.

The flow pattern observations which are to be reported were used to determine the variation in secondary vortex size for a number of fluids over a range of volumetric

Table 2. Experimental Conditions for Study of Secondary Vortex Characteristics

Fluid	n	K ($Nt\ s^n/m^2$)	Shear rate (s^{-1})	N_{Re}'	N_{WS}
A. 4:1 contraction					
F3	.359	5.22	49-1470	0.42-108	0.257-0.673
F4	.479	1.28	41-573	1.3-71	0.155-0.325
F5	.378	2.70	86-1180	1.9-134	0.331-0.723
F6	.366	3.90	52-1310	0.60-118	0.277-0.773
F7	.367	4.75	61-2051	0.63-197	0.258-0.721
F8	.378	4.35	51-1704	0.54-161	0.217-0.632
F9	.391	4.14	50-797	0.55-48	0.206-0.487
F10	.407	3.71	4.7-650	0.18-29	0.148-0.396
F11	.355	7.51	128-2120	1.4-142	0.262-0.575
F12	.333	11.9	54-1170	0.21-70	0.214-0.529
F13	.430	3.94	48-2550	0.55-280	0.125-0.282
B. 2:1 contraction					
F1	.391	4.64	8.9-480	0.10-60	0.145-0.420
F2	.361	7.35	4.3-418	0.02-32	0.102-0.367
F3	.359	5.22	8.5-384	0.08-38	0.122-0.458
F4	.479	1.28	9.2-155	0.52-40	0.101-0.210
F5	.378	2.70	19-281	0.12-34	0.145-0.470
F6	.366	3.90	9.1-305	0.08-38	0.123-0.483

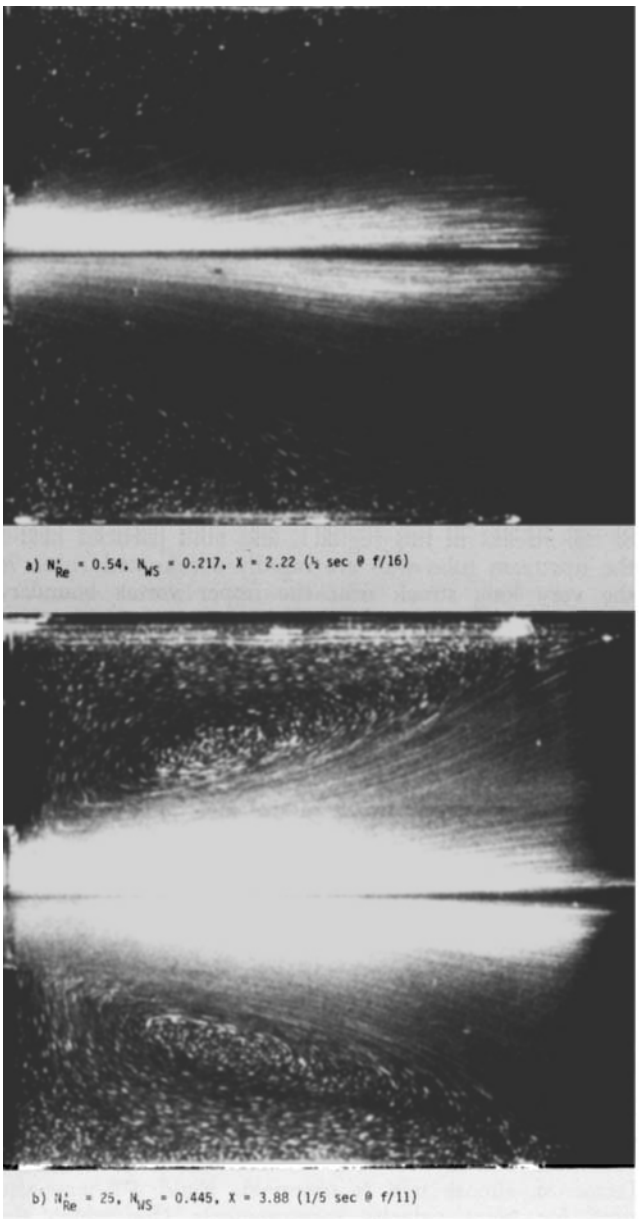

Fig. 7. Flow patterns upstream of the 4:1 contraction for fluid F9 at (*a*) 10.3 cm³/s and (*b*) 109 cm³/s.

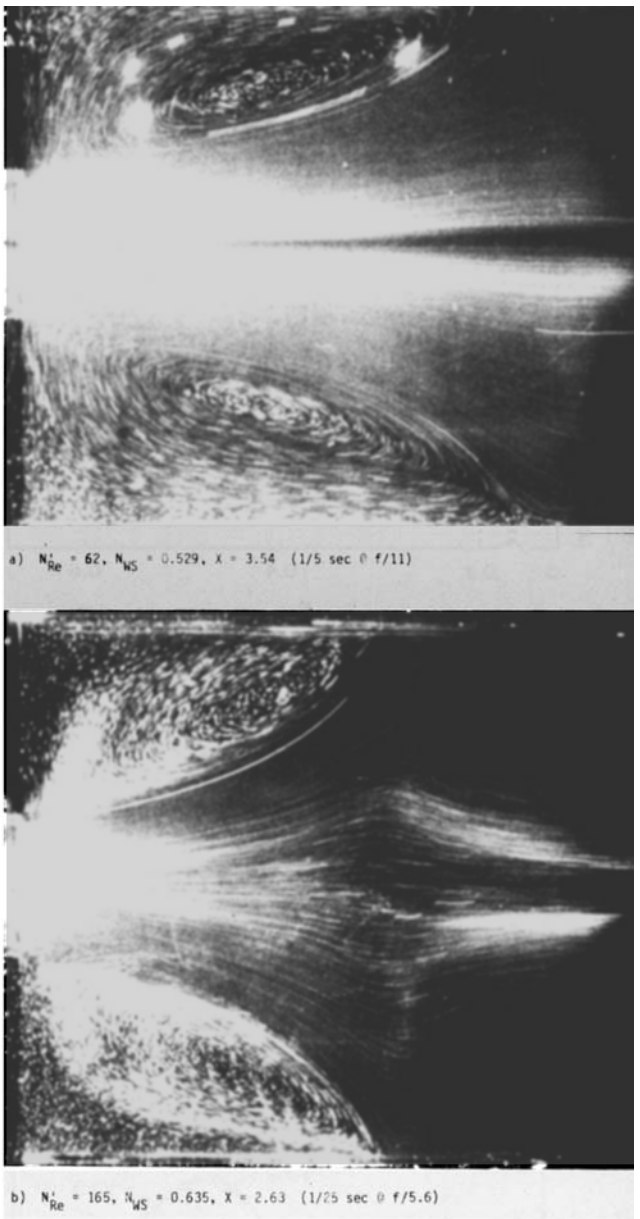

Fig. 8. Flow patterns upstream of the 4:1 contraction for fluid F9 at (*a*) 192 cm³/s and (*b*) 350 cm³/s.

flow rates. From these relatively simple measurements, much may be discovered about the factors influencing the stable entry flow behavior of viscoelastic fluids.

Experimental Conditions

The range of experimental conditions for the vortex characteristics study is summarized for the thirteen fluids used in Table 2. Also shown are the power law parameters n and K which fit the shear stress data over the majority of the experimental shear rate range. They have been included to show the variation in shear thinning characteristics of the test fluids. The power law index n varied by only $\pm 20\%$, whereas the consistency factor K varied by a factor of 10. The test fluids may be considered to have similar shear thinning properties but different viscosity levels. In addition, there was a considerable variation in the level of fluid elasticity, particularly at shear rates above 30 s^{-1}. The values for N'_{Re} and N_{WS} quoted in Table 2 are based on fully developed flow conditions at the wall of the downstream tube. A very large range of values for these parameters was studied, as a result of the significant variation in viscosity and elasticity levels in the fluids used. The vortex length was determined as a function of N'_{Re} and N_{WS} for each fluid over the range of conditions given in Table 2. The vortex detachment length L_V (Figure 6) may be expressed in dimensionless form by

$$X = \frac{L_V}{2R_u} \tag{5}$$

Vortex Characteristics in 4:1 Contraction

Sample streak photographs in Figures 7 and 8 illustrate the stable flow patterns upstream of the 4:1 contraction for fluid F9 at four different flow rates. The photographs show a cross-sectional view of the flow field, fluid flow occurring from right to left in the picture.

At low flow rates, Figure 7*a* shows the presence of a secondary vortex in the 90 deg corner just upstream of the contraction plane. The bulk flow converges smoothly

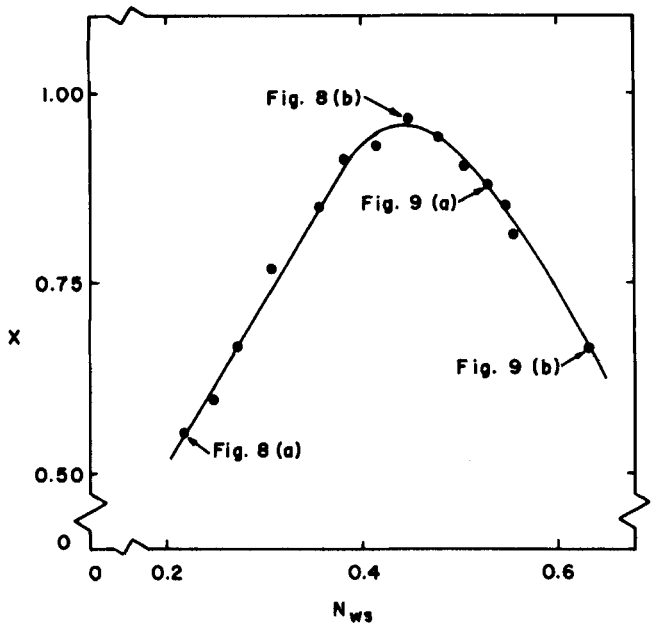

Fig. 9. Dimensionless vortex length vs. N_{ws} for fluid F9 in the 4:1 contraction, showing conditions for Figures 8 and 9.

into the downstream tube with the vortex forming a natural funnel shaped region for flow development. Figure 7*b* shows that the vortex grows in size with increasing flow rate, N'_{Re} increasing from 0.54 to 25, N_{WS} from 0.22 to 0.45. The vortex detachment length increased by 75%.

With further increase in throughput past the conditions of Figure 7*b*, the nature of the entry flow patterns changes, as shown in Figure 8 for N'_{Re} = 62 and 165 and N_{WS} = 0.53 and 0.64. Streak lines near the upstream tube center line begin to diverge out towards the tube wall as the vortex detachment plane is approached, and the vortex size is reduced. The effect becomes very pronounced at the higher flow rate. Figure 8*b* shows that

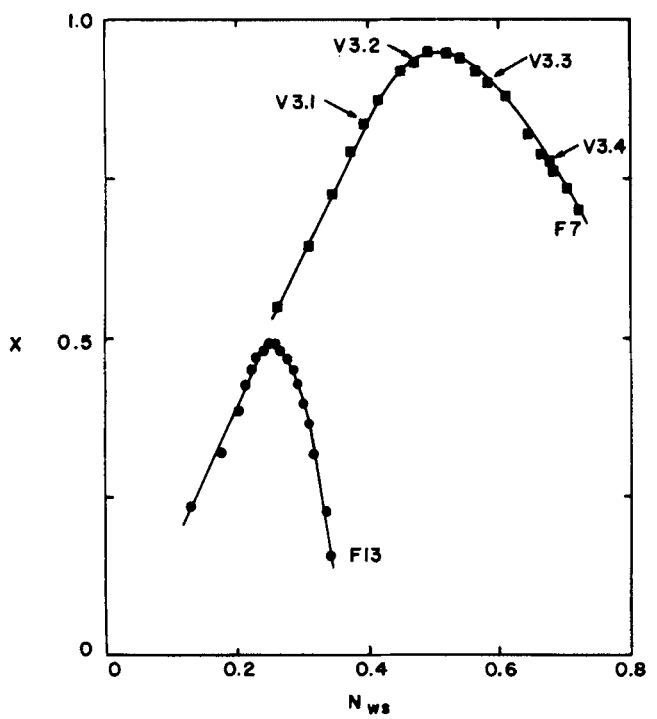

Fig. 11. Dimensionless vortex length vs. N_{ws} for fluids F7 and F13 in the 4:1 contraction, showing also conditions for velocity measurements with fluid F7(V3).

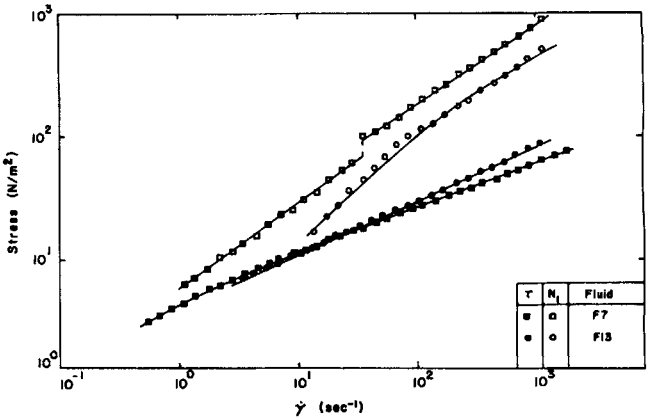

Fig. 10. First normal stress difference and shear stress vs. shear rate for fluids F7 and F13.

deceleration occurs near the center line (note the length of the streaks in this region), and fluid particles nearer the upstream tube wall are rapidly accelerated (observe the very long streak near the upper vortex boundary in Figure 8*b*).

Figure 9 illustrates the vortex characteristics for fluid F9, as dimensionless vortex length vs. N_{WS}, showing the conditions at which the streak photographs of Figures 7 and 8 were obtained. The pronounced vortex growth region is very clearly defined for $0.22 \leq N_{WS} \leq 0.45$. Equally well defined is the behavior at higher flow rates where the vortex decreases in size and the flow diverges upstream of the vortex detachment plane.

The dominant role of fluid elasticity in determining the vortex characteristics may be established by comparing the behavior of two fluids with similar viscosity but different elasticity. Figure 10 shows the variation of shear stress and first normal stress difference with shear rate for fluids F7 and F13. The shear stress behavior is very similar, but fluid F7 is significantly more elastic, the first normal stress difference being up to 80% larger than that for F13. In Figures 11 and 12, the vortex characteristics for the two fluids are compared as vortex length vs. N_{WS} and N'_{Re}, respectively. For the more elastic fluid F7, a vortex size increase by a factor of almost two is observed. Fluid F7 was also used for point velocity measurements (for which the code is V3), and the conditions at which the velocity profiles were measured are indicated in Figure 11. These results will be discussed in Part II.

The creeping flow limit of vortex size for an inelastic Powell-Eyring fluid may be estimated from the results of Duda and Vrentas (1973). Their study indicated that

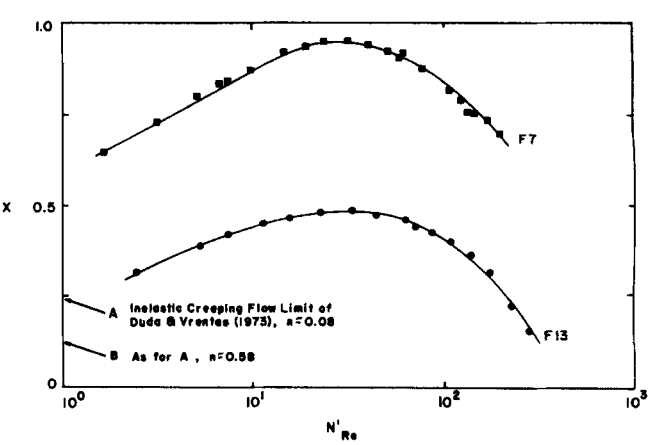

Fig. 12. Dimensionless vortex length vs. N_{Re}' for fluids F7 and F13 in the 4:1 contraction.

the size of secondary vortices in the creeping flow of inelastic fluids through abrupt contractions is enhanced in highly shear thinning fluids. An approximate correspondence between the Powell-Eyring model and the power law model may be obtained by comparing the center-line velocity in fully developed flow. For the most pseudoplastic fluid model used by Duda and Vrentas (equivalent $n \simeq 0.08$), the dimensionless vortex length for $\beta = 4$ was estimated from streamline contours to be $X = 0.24$. For the least pseudoplastic model ($n \simeq 0.58$), the inelastic creeping flow limit was $X = 0.125$. These two values are shown in Figure 12 as A and B, respectively. Increasing N'_{Re} for a purely viscous fluid would cause the vortex to diminish in size from these creeping flow limits. For the less elastic fluid F13, the vortex size approaches the upper inelastic limit for low N'_{Re}. The creeping flow asymptote for F13, ($n = 0.43$), based on consideration of shear thinning effects only, is probably closer to limit $B(n \simeq 0.58)$ than $A(n \simeq 0.08)$. The predominant contribution to the vortex size cannot be attributed to shear thinning and must be a manifestation of the fluid's elasticity.

It is clear from the results presented for fluids F7 and F13 that the level of fluid elasticity has a dominant effect on the secondary vortex length. Two distinct regions exist. For low throughputs, the vortex size is an increasing function of flow rate, and the bulk flow converges smoothly through the funnel shaped vortex region. This flow regime may be termed the vortex growth regime. As the flow rate increases, the vortex size reaches a maximum. At higher throughputs, the vortex decreases in size with increasing flow rate and the flow diverges away from the center line, upstream of the vortex detachment plane. This may be termed the divergent flow regimes. The conditions at which the maximum in vortex size occurs are of considerable significance as will be discussed in Part III.

The combined vortex characteristics data for the eleven fluids studied in the 4:1 contraction are presented in Figure 13 as dimensionless vortex length against N_{WS}. There is no single functional relationship between these parameters, except in the vortex growth regime, where the dashed line indicates direct proportionality between X and N_{WS}. This suggests the plot shown in Figure 14, where N_{WS}/X is graphed against N'_{Re} for all eleven fluids examined in the 4:1 contraction. This relatively simple data reduction has combined all the vortex characteristics data into effectively a single functional relationship. At low N'_{Re}, the quantity N_{WS}/X is substantially constant and independent of N'_{Re}. This corresponds to what has been termed the vortex growth regime. In this region, the nature of the entry flow patterns is completely determined by the ratio of elastic to viscous forces (N_{WS}) and is not affected by changes in fluid inertia; that is, purely rheological forces dominate the entry flow behavior. At higher Reynolds numbers, where fluid inertia begins to have an effect, the vortex characteristics change to the divergent flow regime, and the parameter N_{WS}/X becomes an increasing function of N'_{Re}.

The parameter N_{WS}/X may be interpreted as a macroscopic Deborah number. For Eulerian steady flows, such as the one under consideration, the Deborah number can be defined by

$$N_{De} = \frac{\theta V}{L} \tag{6}$$

N_{WS}/X may be expressed as

$$\frac{N_{WS}}{X} = \beta \frac{\theta \langle v_z \rangle d}{L_v} \tag{7}$$

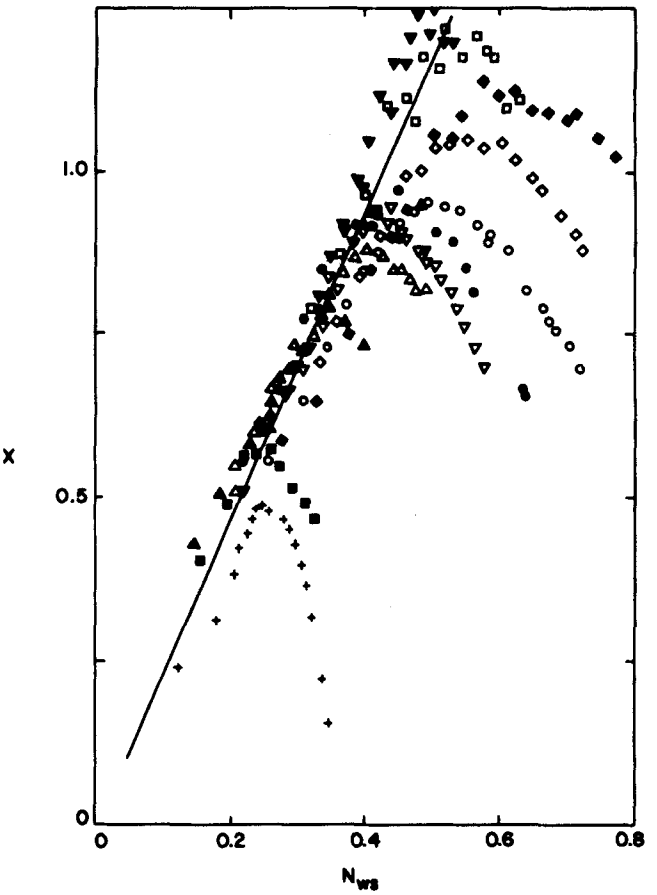

Fig. 13. Dimensionless vortex length vs. N_{ws} for fluids studied in 4:1 contraction.

which is equivalent to the definition in the previous equation, since L_v is a characteristic length in the direction of flow. Thus, the vortex growth regime is a flow regime of constant, small Deborah number. For divergent flow, the Deborah number increases rapidly with N'_{Re} (see Figure 14).

Vortex Characteristics in 2:1 Contraction

Using identical techniques to those described above, the vortex characteristics in 2:1 contraction were determined for the six fluids detailed in Table 2. Similar

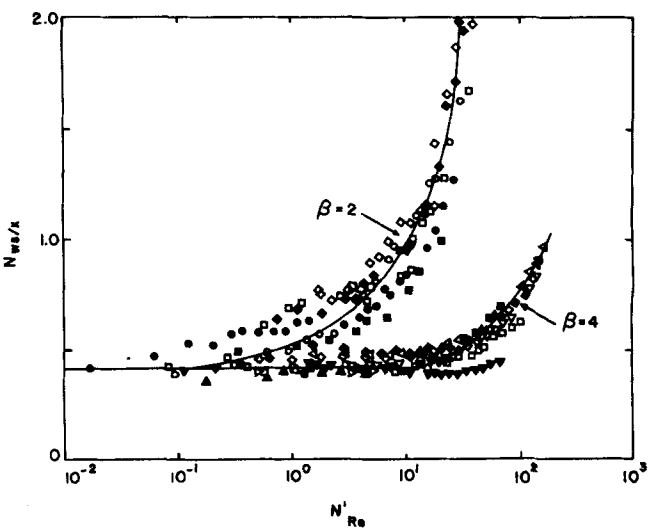

Fig. 14. N_{ws}/X vs. N_{Re}' for all test fluids in both 2:1 and 4:1 contraction.

effects to the 4:1 contraction were observed, except that the vortex was of a significantly smaller volume. This was thought to be due to the smaller acceleration in the lower contraction ratio which leads to less significant effects due to fluid elasticity. Streak photographs of the flow patterns upstream of the 2:1 contraction are available (Cable, 1976). Similar trends are observed as in the 4:1 contraction. and a vortex growth region and diverging flow region can be clearly identified.

The combined vortex characteristics for all fluids in both contractions are shown in Figure 14 as N_{WS}/X vs. N'_{Re}. Despite the scatter in the 2:1 results, it can be concluded definitely that the two contractions give the same asymptotic value for N_{WS}/X at low N'_{Re}. That is, for both the 2:1 and the 4:1 contraction

$$\lim_{N'_{Re} \to 0} \left(\frac{N_{WS}}{X} \right) = 0.40 \qquad (8)$$

This is a very important observation. It indicates that upstream boundary effects on the entry flow patterns reach an asymptotic limit at low Reynolds numbers, and that this is a characteristic of the vortex growth regime. Thus, any realistic theoretical analysis of viscoelastic entry flow which may be carried out in the future should predict this phenomenon, at least in creeping flow. With increasing Reynolds number, deviation of the parameter N_{WS}/X from the creeping flow limit begins at a lower value of N'_{Re} in the 2:1 contraction than in the 4:1 geometry.

An alternative method for reducing the data is to plot X/N'_{Re} against N_{WS}/N'_{Re}. The first parameter is suggested by the approach taken in inelastic boundary-layer theory for normalizing the axial coordinate. The second parameter represents the ratio of elastic to inertial forces. It decreases in magnitude with increasing flow rate. Figure 15 shows the vortex data for the two contractions presented in this way. Over three and a half decades of the independent variable and three decades of the dependent variable, for thirteen fluids in two geometries, for $0.33 < n < 0.48$, $0.02 < N'_{Re} < 280$, and $0.10 < N_{WS} < 0.77$, a good correlation is obtained. At high values of N_{WS}/N'_{Re}, corresponding to low flow rates, the data for the two contractions merge, as expected from Figure 14. At low N_{WS}/N'_{Re}, the data are separated by a horizontal shift factor of two, which equals the ratio of the two contraction ratios. Replotting the data at high flow rate (high N'_{Re}) as X/N'_{Re} against $\beta \cdot N_{WS}/N'_{Re}$ would result in superposition of the data for the two geometries. The data at the low flow rates would not coincide if this technique were used.

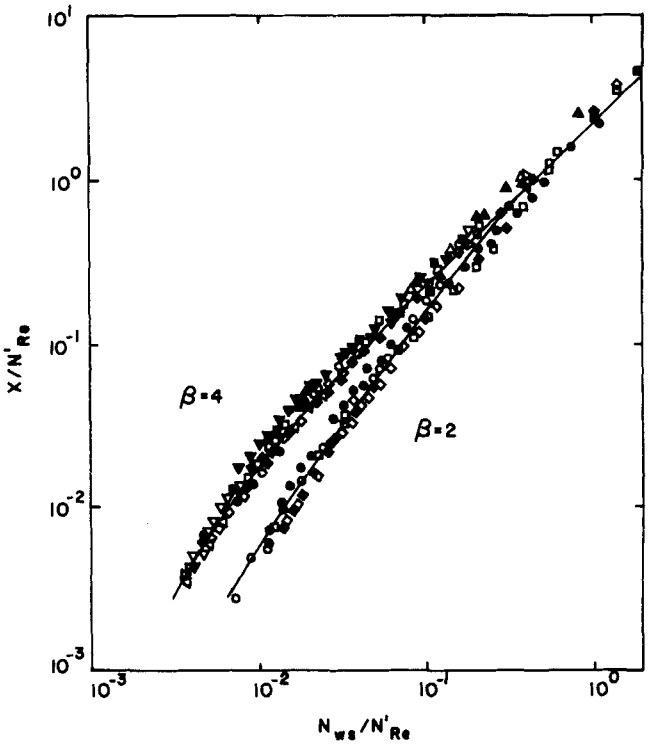

Fig. 15. X/N_{Re}' vs. N_{WS}/N_{Re}' for all test fluids in both 2:1 and 4:1 contractions.

CONCLUSION

The experiments described have enabled the identification of two distinct flow regimes, the vortex growth and divergent flow regimes. Vortex growth is characterized by a smoothly convergent entrance flow and an apparent independence of the flow patterns from inertial effects. In divergent flow, fluid particles near the center line decelerate as the detachment plane is approached, and the vortex decreases in size with increasing throughput. This may be interpreted as an inertial effect.

In the vortex growth regime, the characteristic wine glass stem entry pattern has been observed for both polymer melts and solutions in entry flow. These studies have been discussed in review articles mentioned earlier. The growth of vortex size with throughput has been conclusively shown although not quantified by Ballenger and White (1971) for polymer melts and by Giesekus (1968) and RamaMurthy (1974) for polyacrylamide solutions in abrupt entry flow. It is clear that similar mechanisms are operating for both the melts and solutions in the vortex growth regime. Rheological forces dominate the flow. The characteristics of divergent flow which have been established here have not been reported before for either melts or solutions. Neither has the growth of the vortex been quantified before. However, a recent theoretical analysis (Crochet and Pilate, 1976) for plane entry flow of a second order fluid (no memory effects) has predicted that for Reynolds numbers less than ten, the vortex increases in size when the Weissenberg number increases, while at $N'_{Re} = 100$, the vortex size decreases as Weissenberg number increases. This analysis is in qualitative agreement with the results presented here.

A mechanism for the development and growth of the secondary vortices in abrupt entry regions may be tentatively suggested. Giesekus (1968) presented photographs of flow from a very large reservoir into a slit, where the effect of the upstream reservoir walls was insignificant. The streak photographs clearly demonstrated that the origin of the initial vortex development was the sharp corner at the slit entrance. The vortices were seen to grow, in a direction perpendicular to the center line, as the flow rate increased. In the geometry used in this work, the upstream tube walls restrict the outward growth of the vortices, resulting in an increase in vortex detachment length with flow rate to enable an increase in the overall secondary vortex volume. This qualitative approach is supported by the concurrence of the creeping flow asymptotes for the vortex characteristics in the two geometries used in this study.

ACKNOWLEDGMENT

The experimental measurements for this paper were made in the Department of Chemical Engineering, Monash University, where the work was supported by a grant from the Australian Research Grants Commission. The paper was compiled at the Department of Chemical Engineering, University of Delaware,

where encouragement and helpful suggestions were made by Professors Denn and Metzner. The authors are particularly grateful for this help.

NOTATION

D = downstream tube diameter
K = consistency factor in power law model $\tau = K\dot{\gamma}^n$
L = characteristic length in direction of flow
L_v = length of vortex region
n = flow behavior index in power law model
N_1 = first normal stress difference (P_{11}-P_{22})
N_{De} = Deborah number
N'_{Re} = modified Reynolds number
N_{WS} = Weissenberg number
R_d = radius of downstream tube
R_u = radius of upstream tube
R_v = radius of converging flow region
S = stress ratio
V or $\langle v_z \rangle_d$ = average velocity in downstream tube
X = dimensionless length of vortex region

Greek Letters

β = contraction ratio
$\dot{\gamma}$ = shear rate
ρ = fluid density
τ = shear stress
θ = Maxwell relaxation time

LITERATURE CITED

Atkinson, B., Z. Kemblowski, and J. M. Smith, "Measurements of Velocity Profiles in Developing Liquid Flows," *AIChE J.*, **13**, No. 1, 17-20 (1967).

Bagley, E. B., and A. M. Birks, "Flow of Polyethylene into a Capillary," *J. Appl. Phys.*, **31**, No. 3, 556-561 (1960).

Bagley, E. B., and H. P. Schreiber, "Effect of Die Entry Geometry on Polymer Melt Fracture and Extrudate Distortion," *Trans. Soc. Rheol.*, **5**, 341 (1961).

Ballenger, T. F., and J. L. White, "An Experimental Study of Flow Patterns, in Polymer Fluids in the Reservoir of a Capillary Rheometer," *Chem. Eng. Sci.*, **25**, 1191-1195 (1970).

———, "The Development of the Velocity Field in Polymer Melts in a Reservoir Approaching a Capillary Die," *J. Appl. Polymer Sci.*, **15**, 1949-1962 (1971*a*).

Ballenger, T. F., I. J. Chen, J. W. Crowder, G. E. Hagler, D. C. Bogue, and J. L. White, "Polymer Melt Flow Instabilities in Extrusion: Investigation of the Mechanism and Material and Geometric Variables," *Trans. Soc. Rheol.*, **15**, No. 2, 195-215 (1971*b*).

Boger, D. V., and A. V. RamaMurthy, "Flow of Viscoelastic Fluids Through an Abrupt Contraction," *Rheol. Acta.*, **11**, 61-69 (1972).

Boger, D. V., and P. J. Cable, "An Anomalous Effect in the Measurement of Normal Stress in Polyacrylamide Solutions," *ibid.*, **16**, 322-323 (1977).

Boles, R. L., H. L. Davis, and D. C. Bogue, "Entrance Flows of Polymeric Materials: Pressure Drop and Flow Patterns," *Polymer Eng. Sci.*, **10**, No. 1, 24-31 (1970).

Busby, E. T., and W. C. Macsporran, "An Experimental Study of Non-Rheometric Flows of Viscoelastic Fluids, 1. "Flow into a Re-entrant Tube," *J. Non-Newtonian Fluid Mech.*, **1**, 71-82 (1976).

Cable, P. J., "Laminar Entry Flow of Viscoelastic Fluids," Ph.D. thesis, Monash Univ., Clayton, Victoria, Australia (1976).

Chen, I. Jen, "A Comparative Study of Rheological Models for Polymer Melts," Ph.D. thesis, Univ. Tenn. (1971).

Clegg, P. L., "The Flow Properties of Polyethylene and their Effect on Fabrication," *Trans. J. Plast. Inst.*, **26**, (64) 151-171 (1958).

Coulter, P. R., "A Computer Program for Non-Linear Regression Analysis and Function Minimization," *Rept. No. CHER 70-2, Dept. of Chem. Eng.*, Monash Univ., Clayton, Victoria, Australia (1970).

Crochet, M. J., and G. Pilate, "Plane Flow of a Fluid of Second Grade Through a Contraction," *J. Non-Newtonian Fluid Mech.*, **1**, 247-258 (1976).

Dennison, M. T., "Flow Instability in Polymer Melts: A Review," *Trans. J. Plast. Inst.*, **35**, 803-808 (1967).

Duda, J. L., and J. S. Vrentas, "Entrance Flows of Non-Newtonian Fluids," *Trans. Soc. Rheol.*, 89-108 (1973).

Giesekus, H., "Non-Linear Effects in the Flow of Viscoelastic Fluids Through Slits and Circular Apertures," (in German), *Rheol. Acta*, **7**, No. 2, 127-138 (1968).

Halmos, A. L., "The Flow of Viscous and Viscoelastic Fluids Through an Abrupt Expansion," Ph.D. thesis, Monash Univ., Clayton, Victoria, Australia (1973).

Han, C. D., and L. H. Drexler, "Studies of Converging Flows of Viscoelastic Polymeric Melts III Stress and Velocity Distributions in the Entrance Region of a Tapered Slit Die," *J. Appl. Polymer Sci.*, **17**, 2369-2393 (1973).

Insarova, N. I., "Photoelastic Investigation of the Flow Instability of a Polystyrene Melt," *Polymer Mechanics*, **5**, No. 3, 487-490 (1969).

Kearsley, E. A., "A Test Sample to Standardize Measurements of Normal Stress," *Rheol. Acta*, **12**, 546-549 (1973).

———, Private communication (1974).

Metzner, A. B., E. A. Uebler and C. F. Chan Man Fong, "Converging Flows of Viscoelastic Materials," *AIChE J.*, **15**, No. 5, 750-758 (1969).

Oliver, D. R., and R. Bragg, "Flow Patterns in Viscoelastic Liquids Upstream of Orifices," *Can. J. Chem. Eng.*, **51**, 287-290 (1973).

Den Otter, J. L., "Mechanisms of Melt Fracture," *Plastics and Polymers*, **38**, 155-168 (1970).

Oyanagi, Y., "A Study of Irregular Flow Behavior of High Density Polyethylene," *Appl. Polymer Symposium No. 20*, 123-126 (1973).

Pearson, J. R. A., and T. J. F. Pickup, "Stability of Wedge and Channel Flow of Highly Viscous and Elastic Liquids," *Polymer*, **14**, 209-214 (1973).

Perera, M. G. N., and K. Walters, "Long Range Memory Effects in Flows Involving Abrupt Changes in Geometry Part 1: Flows Associated with L-Shaped and T-shaped Geometrics and Part 2: The Expansion/Contraction/Expansion Problem," *J. Non-Newtonian Fluid Mech.* (1977).

Petrie, C. J. S., and M. M. Denn, "Instabilities in Polymer Processing," *AIChE J.*, **22**, No. 2, 209-236 (1976).

RamaMurthy, A. V., "Laminar Flow of Viscous and Viscoelastic Fluids in the Entrance Region of a Pipe," Ph.D. thesis, Monash Univ., Clayton, Victoria, Australia (1970).

———, "Flow Instabilities in a Capillary Rheometer for an Elastic Polymer Solution," *Trans. Soc. Rheol.*, **18**, No. 3, 431-452 (1974).

Schott, H. and W. S. Kaghan, "Flow Irregularities in the Extrusion of Polyethylene Melts," *Ind. Eng. Chem.*, **51**, 844-846 (1959).

Southern, J. H., and D. R. Paul, "Elastic Fracture of Polystyrene Solutions," *Polymer Eng. Sci.*, **14**, No. 8, 560-566 (1974).

Strauss, K., and R. Kinast, "Secondary Flow Effects in the Flow of Viscoelastic Fluids Through Wedge-Shaped Dies," (in German), *Colloid Polymer Sci.*, **252**, No. 9, 753-758 (1974).

Tomita, Y., and T. Shimbo, "Unstable Flow of Viscoelastic Fluids," *Appl. Polymer Symposium No. 20*, 137-153 (1973).

Tordella, J. P., "Capillary Flow of Molten Polyethylene—A Photographic Study of Melt Fracture," *Trans. Soc. Rheol.*, **1**, 203-212 (1957).

———, "Unstable Flow of Molten Polymers—A Second Site of Melt Fracture," *J. Appl., Polymer Sci.*, **7**, 215-229 (1963).

Vinogradov, G. V., and V. N. Manin, "An Experimental Study of Elastic Turbulence," *Kolloid Z. -Z. Polymere*, 201, 93-98 (1964).

Vinogradov, G. V., N. I. Insarova, B. B. Boiko, and E. K. Bortsenkova, "Critical Regimes of Shear in Linear Polymers," *Polymer Eng. Sci.*, **12**, No. 5, 323-334 (1972).

Walters, K., *Rheometry*, Chapman and Hall, London, England (1975).

White, J. L., "Critique on Flow Patterns in Polymer Fluids at the Entrance of a Die and Instabilities Leading to Extrudate Distortion," *Appl. Polymer Symposium No. 20*, 155-174 (1973).

Manuscript received April 4, 1977; revision received March 14, and accepted March 27, 1978.